Progress In Electromagnetics Research, Vol. 141, 185–200, 2013

ARTIFACT REMOVAL ALGORITHMS FOR MICROWAVE IMAGING OF THE BREAST

Muhammad A. Elahi*, Martin Glavin, Edward Jones, and Martin O'Halloran

College of Engineering and Informatics, National University of Ireland Galway, Galway, Ireland

Abstract—One of the most promising alternative imaging modalities for breast cancer detection involved the use of microwave radar systems. A critical component of any radar-based imaging system for breast cancer detection is the early-stage artifact removal algorithm. Many existing artifact removal algorithms are based on simplifying assumptions about the degree of commonality in the artifact across all channels. However, several real-world clinical scenarios could result in greater variation in the early-stage artifact, making the artifact removal process much more difficult. In this study, a range of existing artifact removal algorithms, coupled with algorithms adapted from Ground Penetrating Radar applications, are compared across a range of appropriate performance metrics.

1. INTRODUCTION

In the context of early breast cancer detection, Confocal Microwave Imaging (CMI) has been proposed as a method to identify and locate regions of dielectric scatterings within the breast [1, 2]. Adaptive beamforming is typically used to process the backscattered signals, and to compensate for frequency-dependent propagation effects [3–5]. Regions of high energy within the resultant images may suggest the presence of cancerous tissue due to the dielectric contrast that exists between normal and cancerous tissue. Other approaches such as Microwave Tomography, reconstruct the spatial distribution of dielectric properties within the breast, using inverse scattering algorithms [6, 7].

One of the most important components of any CMI system for breast cancer detection is the early-stage artifact removal algorithm.

Received 24 May 2013, Accepted 6 July 2013, Scheduled 12 July 2013

* Corresponding author: Muhammad Adnan Elahi (m.elahi1@nuigalway.ie).

The early-stage artifact is composed of the input signal, the reflection from the skin-fat interface and any antenna reverberation present. This artifact is typically several orders of magnitude greater than the reflections from any tumours present within the breast. If the artifact is not removed effectively, it could easily mask tumours present within the breast. Despite the importance of artifact removal, and the development of a number of algorithms, no comprehensive comparison of early-stage artifact removal algorithms for breast cancer detection using microwave imaging has been performed previously. In this paper, a wide-range of existing microwave breast imaging artifact removal algorithms, along with algorithms adapted from Ground Penetrating Radar (GPR) applications, are implemented and compared across a range of appropriate performance metrics. The remainder of the paper is organised as follows: Section 2 describes each artifact removal algorithm in detail; Section 3 describes the numerical breast phantom and performance metrics used to evaluate the algorithms; Section 4 describes the various tests applied to the artifact removal algorithms and the corresponding results; Finally, conclusions and suggestion for possible future work are discussed in Section 5.

2. ARTIFACT REMOVAL ALGORITHMS

2.1. Average Subtraction

In this simple method, the artifact is estimated as an average of the signal recorded at each channel. The artifact is removed by subtracting this estimated artifact from each received signal:

$$s_i[n] = b_i[n] - \frac{1}{N}\sum_{i=1}^{N} b_i[n] \tag{1}$$

where $b_i[n]$ is the vector containing the signal recorded at channel n, N is the total number of channels and $s_i[n]$ is the artifact-free signal.

2.2. Rotation Subtraction

The Rotation Subtraction method was proposed by Klemm et al. [8] and requires two separate radar measurements. The first set of measurements is recorded with the circular antenna array surrounding the breast in one position and a second set of signals is recorded after the antenna array has been rotated at a certain angle in the horizontal plane around the vertical axis, as follows:

$$s_i[n] = b_i[n] - b_r[n] \tag{2}$$

where $b_r[n]$ is the vector containing the signals recorded after the antenna array has been rotated.

2.3. Adaptive Filtering

2.3.1. Wiener Filter

The Wiener Filter artifact removal algorithm was originally proposed by Bond et al. [3]. This algorithm improves on the simple Average Subtraction method by compensating for channel-to-channel variation in artifacts due to local variation in skin thickness, breast heterogeneity and differences in antenna-skin distances. In this method, the artifact in each channel is estimated as a filtered combination of the signals in all other channels. The estimated artifact signal for channel i is then subtracted from the received signal at channel i as follows:

$$s_i[n] = b_i[n] - q^T b_{PN}[n] \tag{3}$$

where $b_i[n]$ is the vector containing the signal received at channel i, $b_{PN}[n]$ a vector calculated from all other channels except i, and q the vector of filter weights. The filter weights are chosen to minimize the residual signal mean-squared error over the portion of the signal dominated by the artifact.

For example, in order to remove the artifact from channel 1, a $(2J+1) \times 1$ vector of time samples in the kth channel is defined as:

$$b_k[n] = [b_k[n-J], \ldots, b_k[n], \ldots b_k[n+J]]^T, \quad 2 \le k \le N \tag{4}$$

where J is the number of samples on either side of nth time sample and $2J+1$ the length of the averaging window centered on n. The samples of $b_k[n]$ for channels 2 through N are concatenated into a vector $b_{2N}[n]$ as:

$$b_{2N}[n] = \left[b_2^T[n], b_3^T[n], \ldots, b_N^T[n]\right]^T \tag{5}$$

The filter weight vector q is then calculated as

$$q = \arg\min_q \sum_{n=n_o}^{n_o+m-1} \left|b_1[n] - q^T b_{2N}[n]\right|^2 \tag{6}$$

where the time window $n = n_o$ to $n = n_o + m - 1$ represents the initial portion of the signal dominated by artifact.

2.3.2. Recursive Least Squares Filter

The Recursive Least Squares (RLS) algorithm was proposed for artifact removal by Sill et al. [9]. RLS is an adaptive filtering algorithm that recursively computes and updates the filter weights, in contrast to the

Wiener Filter method which shifts constant weight vectors through the selected window. Let u_r be the $1 \times N$ vector containing N time samples of desired signal at channel r and $u = [u_{r+1}, u_{r+2}, \ldots, u_{r+Q}]^T$ is the $Q \times N$ matrix containing signals at the remaining Q channels. Define $Q \times 1$ weight vector at time n is:

$$w(n) = [w_{r+1}(n), w_{r+2}(n), \ldots, w_{r+Q}(n)]^T \tag{7}$$

The desired signal $d(i) = u_r$ can then be approximated as:

$$\hat{d}(i) = w^T(n)u(i) \tag{8}$$

and the error is calculated as:

$$e(i) = d(i) - \hat{d}(i) \tag{9}$$

At time n the sum of squared error is defined as:

$$J(n) = \sum_{i=1}^{n} \lambda^{n-i} |e(i)|^2 \tag{10}$$

where λ is the forgetting factor and n the current sample number. The minimization of mean squared error with respect to $w(n)$ results in the well-known Wiener-Hopf equation which can be recursively solved using standard brute force approach. Further details on the specific implementation can be found in [9]. The RLS algorithm is used in conjunction with Woody-Averaging [10]. The RLS algorithm is applied to the initial portion of signal which is dominated by artifact and Woody averaging is applied to remaining portion of the signal. This total estimated signal is then subtracted from the target signal. The artifact-dominated portion of signal is selected empirically in this study.

2.3.3. Singular Value Decomposition

Singular Value Decomposition (SVD) has been previously used for clutter reduction in GPR [11] and through-wall imaging [12]. SVD is used to decompose the received data into tumour and artifact subspaces. The components containing the tumour are selected, discarding the artifact. The received signals are represented by a $Q \times N$ matrix X where N is the total number of time samples and Q is the total number of channels. A singular value decomposition of X is given as:

$$X = USV^T \tag{11}$$

where $U = [u_1, u_2, \ldots, u_M]$ and $V = [v_1, v_2, \ldots, v_N]$ (having dimensions $Q \times Q$ and $N \times N$) are left and right unitary matrices

respectively. Let $S = \text{diag}(\sigma_1, \sigma_2, \ldots, \sigma_Q)$ with $\sigma_1 \geq \sigma_2 \geq \ldots \geq \sigma_Q \geq 0$ be the singular values of X. The SVD of X can then be written as:

$$X = \sum_{i=1}^{Q} \sigma_i u_i v_i^T \tag{12}$$

$$X = E_1 + E_2 + E_3 + \ldots + E_N \tag{13}$$

where E_i is the ith eigenvalue of the mode of X having the same dimensions as of X.
X can be decomposed into two subspaces as:

$$X = \sum_{i=1}^{k} \sigma_i u_i v_i^T + \sum_{i=k+1}^{Q} \sigma_i u_i v_i^T \tag{14}$$

where the first k singular values belong to the artifacts and the remaining values belong to the tumour response. Verma et al. [12] proposed that first spectral component $k = 1$ in (14) represents the clutter. However, in this study the experimental data suggested that the clutter subspace is composed of more than one spectral component. Therefore, the difference of singular values $\sigma_i - \sigma_{i+1}$ is used to estimate the optimal value of k:

$$k = \arg\max_i(\sigma_i - \sigma_{i+1}) \tag{15}$$

2.4. Entropy Based Time Window

The Entropy Based Time Window artifact removal algorithm was proposed by Zhi and Chin [13]. The algorithm is based on the assumption that the artifacts in the received signals are highly similar across all channels, which is not the case for the tumour response, as it is delayed and attenuated differently in each channel. Entropy is a measure of the variation of the signal, where entropy is inversely proportional to the amount of variation. Therefore, a larger value of entropy is obtained from similar artifacts in the early portion of the radar signal and conversely the tumour reflections result in a much lower entropy value. A window function can be defined based on the entropy values and the artifacts can be removed by multiplying the window function with the received signal at each channel.
A probability density function is created by normalizing each received radar signal:

$$p_i[n] = \frac{\|b_i[n]\|^2}{\sum_{i=1}^{Q} \|b_i[n]\|^2} \tag{16}$$

where $b_i[n]$ is the received signal at ith channel, and Q is the total number of channels. Previous Equation (16) satisfies $p_i[n] \geq 0$ and $\sum_{i=1}^{Q} p_i[n] = 1$ and can be interpreted as energy density in antenna domain. The αth-order Renyi entropy at time sample n is defined as:

$$H_\alpha[n] = \frac{1}{1-\alpha} \log \left\{ \sum_{i=1}^{Q} (p_i[n])^\alpha \right\} \tag{17}$$

where α is real-positive and the entropy varies from zero for certain event to $\log Q$ for uniform distribution. Next $e^{H_\alpha^s[n]}$ is defined as the theoretical dimension of $[b_1[n], b_2[n], \ldots, y_Q[n]]$ where $H_\alpha^s[n]$ is the smoothed entropy, given as:

$$H_\alpha^s[n] = \frac{1}{M} \sum_{k=n}^{k=n+M} H_\alpha[k] \tag{18}$$

The time window function is obtained by comparing the theoretical dimension with a specific threshold as follows:

$$W[n] = \begin{cases} 0, & e^{H_\alpha^s[n]} > N_0 \\ 1, & \text{otherwise} \end{cases} \tag{19}$$

where $1 < N_0 < Q$.
The artifact removed signal can then be obtained by multiplying the time window function with the received signal at the ith channel:

$$s_i[n] = W[n] b_i[n] \tag{20}$$

2.5. Frequency Domain Pole Splitting

The Frequency Domain Pole Splitting artifact removal algorithm was originally proposed by Maskooki et al. [14]. The principle of this algorithm is to represent the frequency response of each received radar signal as a sum of complex exponentials, where each complex exponential represents a pole of the system and each pole corresponds to a specific scatterer in the view of the antenna. The artifacts can then be removed by removing the pole corresponding to the strongest scatterers from frequency response. The frequency response of each received signal can be decomposed into its poles as follows:

$$y(k) = \sum_{p=1}^{N} a_p e^{\left(\alpha_p + j\frac{4\pi}{c} R_p\right) k\Delta f} \tag{21}$$

where N is the total number of scatterers or poles of the system, a_p the constant coefficient, α_p the frequency decay/growth factor, R_p

the range of the pth scatterer, and Δf the sampling frequency. The received signals are first converted to the frequency domain using the Fast Fourier Transform (FFT) algorithm. These frequency domain signals are then processed using the linear system identification method to estimate the frequency model given in (21) [15]. The frequency domain signal is arranged in the form of a Hankel matrix as follows:

$$H = \begin{bmatrix} y_i(1) & \dots & y_i(L) \\ \vdots & \ddots & \vdots \\ y_i(N-L+1) & \dots & y_i(N) \end{bmatrix} \tag{22}$$

where $y_i(n)$ is nth frequency sample at channel i, and N is the total number of frequency samples. The Hankel matrix is then decomposed into the signal plus noise and noise only subspaces using SVD and removing the noise subspace. H can be approximated as:

$$\tilde{H} = U_{sn} \Sigma V_{sn}^* \tag{23}$$

where U_{sn} is the left unitary matrix of the signal-plus-noise subspace, V_{sn}^* the right unitary matrix of signal plus noise subspace, and Σ contains the dominant singular values of H in descending order and $(*)$ denotes conjugate transpose. The criterion to separate the two subspaces is the Akaike Information Criterion [16]. The approximated H from (23) is used to estimate the a_p, α_p and R_p. Using these parameters in (21), the frequency domain signal is reconstructed. The parameter a_p is directly related to the amplitude of pulses in the time domain signal. Since the magnitude of the tumour pulse is much smaller than the artifact, a threshold is used to remove the poles with dominant a_p values during the reconstruction of the frequency response. Hence, the reconstructed signal will only contain the tumour response. This reconstructed signal is then converted into the time domain using the inverse FFT.

3. NUMERICAL BREAST PHANTOM AND PERFORMANCE METRICS

A 2D Finite Difference Time Domain (FDTD) breast model has been developed, based on an MRI-derived breast phantom, taken from the UWCEM breast phantom repository at the University of Wisconsin-Madison [17]. Two breast models have been considered in this study. The FDTD model shown Fig. 1(a) is dielectrically homogeneous model, composed of adipose tissues only whereas the model shown in Fig. 1(b) is heterogeneous with a region of fibroglandular tissue.

The antenna array consists of 12 elements modelled as electric-current sources equally spaced around the circumference of the breast

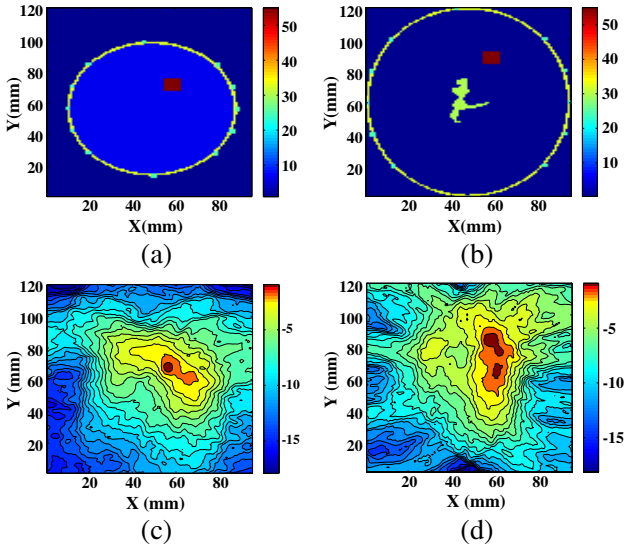

Figure 1. FDTD breast model with antennas and corresponding beamformed images after ideal artifact removal: (a) homogeneous breast model, (b) heterogeneous breast model, (c) beamformed image of homogeneous breast model, (d) beamformed image of heterogeneous breast model.

and backed by a synthetic material matching the dielectric properties of adipose tissue. The entire simulation space is 95 mm × 120 mm. A location within the breast is described in terms of (X mm, Y mm). A 7.5 mm diameter tumour is located at two different positions in each breast model ((59 mm, 72 mm) and (59 mm, 88 mm)). The input signal is a 150-ps differentiated Gaussian pulse, with a centre frequency of 7.5 GHz and a −3 dB bandwidth of 9 GHz. Before further processing, the acquired backscattered recorded signals are downsampled from 1200 GHz to 50 GHz.

Four metrics are used to evaluate the artifact removal algorithms. The Peak-to-peak Response Ratio (PPRR) and Correlation Measure (CM) are applied to the raw radar signals, whereas the Signal-to-Mean Ratio (SMR) and Structure Similarity Index Metric (SSIM) [18] are calculated from the resultant beamformed images.

The PPRR is the ratio of the peak-to-peak magnitude of the radar signal following and prior to artifact removal. The PPRR measures how much of the artifact has been removed from a particular channel. The CM is used to measure the ability of artifact removal algorithm to preserve the tumour response. This is computed by correlating

the ideal tumour response with the tumour response obtained for a particular artifact removal algorithm. The SMR is a measure of the quality of beamformed image after the application of a particular artifact removal algorithm. It is defined as the ratio of peak tumour response to the average response in the image. Finally, the SSIM is an image quality metric, that indicates the similarity between two images. The SSIM outputs a values in the range 0–1, where 1 indicates that the test and the reference image are identical. An ideal reference image is generated using an ideal artifact removal algorithm. SSIM is calculated as follows:

$$\text{SSIM} = \frac{(2 \times \bar{x} \times \bar{y} + C1)\,(2 \times \sigma_{xy} + C2)}{\left(\sigma_x^2 + \sigma_y^2 + C2\right) \times (\bar{x}^2 + \bar{y}^2 + C1)}$$

where x is the reference image; y is the test image; $\bar{x}$ and $\bar{y}$ represent the corresponding mean; σ_x and σ_y represent the corresponding variance; σ_{xy} is the covariance of the reference and test image; $C1$ and $C2$ are small constants.

4. RESULTS

Table 1 illustrates the overall performance of each artifact removal algorithm in terms of PPRR and CM, while Table 2 presents their respective performances in terms of the quality of the resultant breast images (SMR and SSIM). Fig. 2 shows the time-domain plots and images for each algorithm.

From Table 1, the Average Subtraction and Rotation Subtraction algorithms fail to effectively remove the artifact, as indicated by the fact that these algorithms have the lowest PPRR values. The PPRR

Table 1. Performance metrics for artifact removed signals.

Algorithms	PPRR	Correlation Measure
Ideal	−131.39	1.00
Rotation Subtraction	−30.73	0.14
Average Subtraction	−38.18	0.10
Wiener Filter	−126.38	0.66
RLS	−83.61	0.37
SVD	−123.19	0.45
Entropy Based Time Window	−121.88	0.60
Frequency Domain	−135.43	0.37

Table 2. Performance metrics for beamformed images.

Algorithms	SSIM	SMR
Ideal	1.00	30.32
Rotation Subtraction	0.05	15.00
Average Subtraction	0.05	18.38
Wiener Filter	0.84	25.59
RLS	0.80	25.88
SVD	0.72	25.36
Entropy Based Time Window	0.77	24.54
Frequency Domain	0.60	23.07

and CM values for the RLS algorithm suggest that while the algorithm removes the majority of the artifact, the tumour response suffers significant distortion. Similarly, the SVD algorithm also significantly reduced the artifact but introduces distortion in the tumour response. The Entropy Based Time Window performed quite well as evidenced by both the PPRR and CM values. The Frequency Domain Pole Splitting algorithm has better PPRR value but poor CM value, again indicating a distortion of the tumour response. Finally, the Weiner Filter yields a smaller PPRR value and the highest CM value, suggesting that it not only removes almost all the artifact, but it also preserves the tumour response.

Similar trends can be seen in terms the imaging performance metrics shown in Table 2. The Wiener Filter algorithm produces the highest SSIM value indicating that it generated best beamformed image. SSIM values for RLS and Entropy based Window algorithm are also quite close to the ideal image. The RLS algorithm has high SSIM value despite its poor CM value, because residual artifacts have been compensated by beamformer. A more detailed analysis of the performance of each algorithm is now provided.

Figure 2(a) shows the radar signal derived from the homogeneous model, after processing by the Rotation Subtraction artifact removal algorithm, and the same signal following the application of an ideal artifact removal algorithm. The solid line shows the ideal signal and dashed line is the tumour response signal after the Rotation Subtraction algorithm has been applied. The results are obtained after the antenna array has been rotated by 30°. It can be seen that the Rotation Subtraction algorithm has failed to completely remove the artifact. This is due to the variation in artifact at different locations across the breast. Figs. 2(b)–(c) show the images generated from the

resultant artifact removed signals. Maximum energy concentration is at the antenna locations due to dominant artifacts which remain following the application of the Rotation Subtraction algorithm.

Figures 2(d)–(f) illustrate the performance of the simple Average Subtraction artifact removal algorithm. The signals obtained following the application of the Average Subtraction algorithm still have strong artifacts contained in the early-stage response. This can be attributed to the fact that the Average Subtraction algorithm assumes that the early-stage artifact will be same across all channels, and the averaging

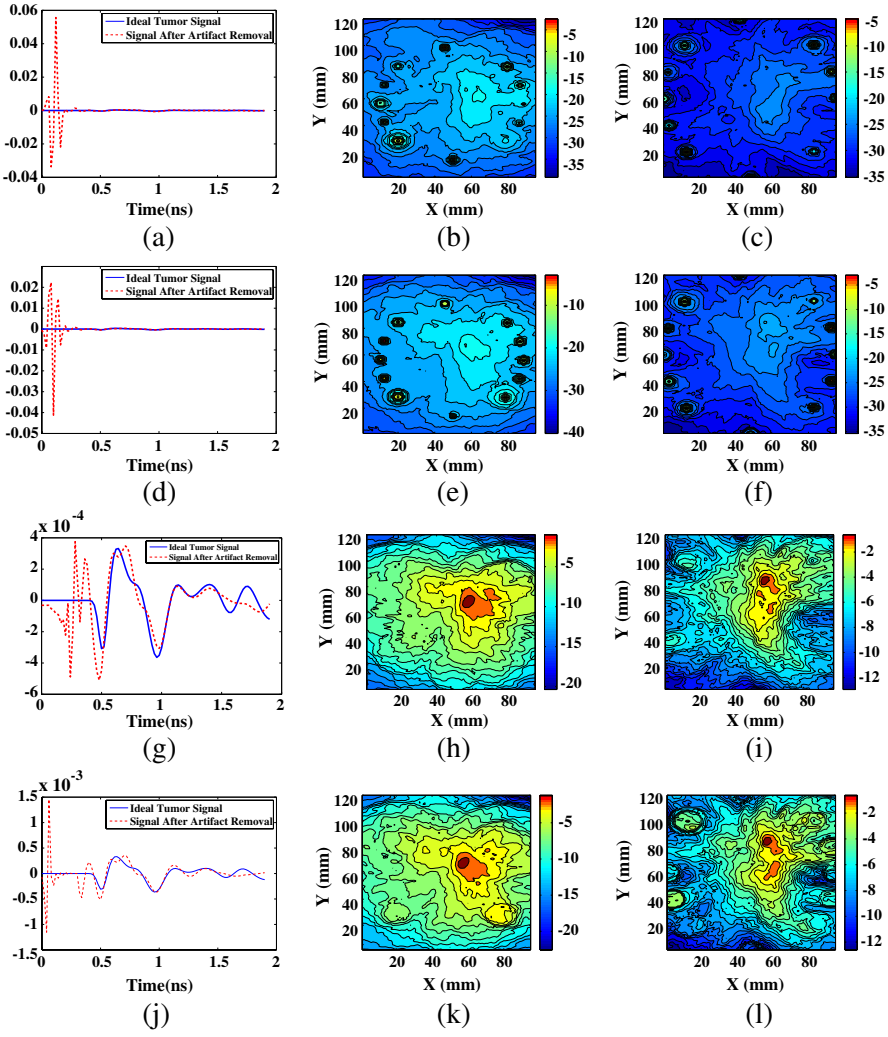

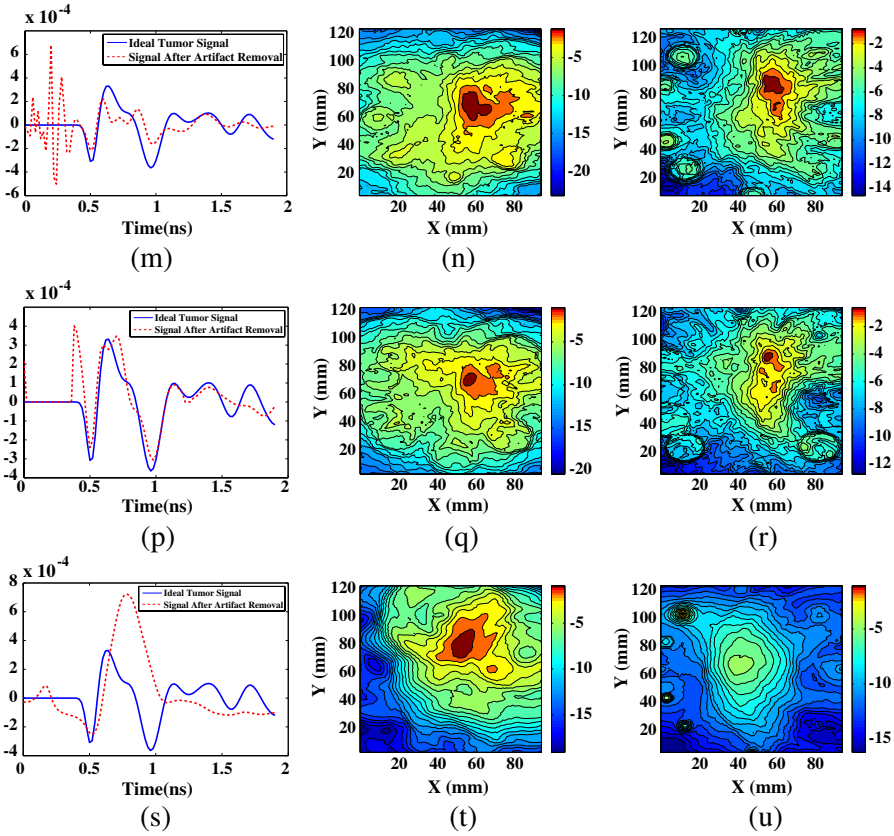

Figure 2. Artifact removed time domain signals and the corresponding beamformed images.

process will correctly estimate the artifact. However, typically the artifact varies between channels due to local variations in skin thickness and differences in the antenna-skin distance. Due to the presence of strong artifacts in the resultant image, the tumour cannot be detected in the breast images, as shown in Figs. 2(e)–(f).

The Wiener Filter artifact removal algorithm is applied to the radar signals with filter parameters $J = 3$, $p = 12$, $m = 23$ and results are plotted in Figs. 2(g)–(i). The results demonstrate that artifacts have been significantly reduced when compared to the Rotation Subtraction and Average Subtraction algorithms. The Wiener Filter algorithm has performed equally well for both tissue models considered in this study. Fig. 2(g) shows that the Wiener Filter algorithm has not been able to completely eliminate the skin artifacts, but they are

significantly reduced with very little distortion being introduced in to the tumour response. The resultant beamformed images are shown in Figs. 2(h)–(i). The images closely resemble the ideal images shown in Figs. 1(c)–(d) and both tumours can be easily detected.

The RLS Filter combined with Woody Averaging artifact removal algorithm is applied to the received signals and results plotted in Figs. 2(j)–(l). These results demonstrate that RLS-Woody combination has reduced the artifacts but residual artifacts still remain. These residual artifacts include a peak in the early-time response which is actually greater in magnitude than the tumour response. Furthermore, the averaging of the late-time signal introduces distortion in the tumour response, which can reduce the quality of the resultant beamformed images. These images are shown in Figs. 2(k)–(l).

Figures 2(m)–(r) show the results obtained by removing the early-stage artifact using SVD. It can be seen that the algorithm has reduced the artifact but failed to completely remove the artifact. It has also significantly distorted the tumour response and this distortion effect is clearly visible in beamformed images, where tumour energy looks relatively dispersed (i.e., incoherent addition of the radar signals at the tumour location), as shown in Figs. 2(m)–(r).

In the case of the Entropy Based Time Window algorithm, third order entropy with $\alpha = 3$ is computed for the received radar signals. The artifact has a large entropy compared to the late-time tumour response. The threshold value is set to half of the number of channels, i.e, $N_0 = 6$ in order to design the time-window (which is then multiplied with radar signals across all channels). This is shown in Fig. 2(p) where the artifacts have been almost completely removed by this algorithm while portions of artifacts close to the tumour response were not removed. This is due to the fact that the algorithm incorrectly estimates the artifact as part of the tumour response when the residual artifacts are very close in magnitude to tumour response. Since the algorithm is only applied to the early-time portion of the signal, no distortion of the tumour response occurs. Images obtained from signals after the Entropy Based Time Window algorithm are applied are shown in Figs. 2(p)–(r).

The Frequency Domain Pole Splitting algorithm is applied to the radar signals and results are shown in Figs. 2(s)–(u). In order to remove the dominant poles, the threshold is set to higher than the ratio of peak tumour to the artifact response multiplied by the maximum a_p values, as proposed by Maskooki [14]. The poles with a_p values larger than this threshold are then removed. The algorithm is quite effective in removing artifacts, but the distortion in the tumour response is much

greater as compared to all other algorithms, resulting in relatively poor images as shown in Figs. 2(s)–(u). Residual artifacts and distortion are much more visible in the hetergeneous model. The tumour can be detected in the homogeneous model as shown in Fig. 2(t) but it is obscured by clutter in the heterogeneous model as shown in Fig. 2(u).

5. CONCLUSIONS AND FUTURE WORK

In this paper, an extensive range of artifact removal algorithms developed originally for both microwave breast imaging and GPR applications have been described and compared. Results presented in this study indicate that the Rotation Subtraction and Average Subtraction artifact removal algorithms fail to effectively remove the early-stage artifact, primarily due to local variations in skin thickness and differences in the antenna-skin distance. Conversely, adaptive filtering algorithms perform well when applied to the portion of signal dominated by artifacts and are more robust to variations in the early-stage artifact. The Frequency Domain Pole Splitting and the SVD method significantly reduce the artifact but tend to introduce considerable distortion in the tumour response. The Entropy Based Time Window algorithm completely removes the part of signal estimated to contain the artifacts; however it often fails to accurately estimate the exact portion of signal containing the artifact.

Future work will focus on the development of a hybrid artifact removal algorithm, where the Entropy Based Time Window algorithm will be improved to better estimate the part of signal containing the artifact and the Wiener Filter algorithm will be used to remove this artifact without introducing any distortion into the tumour response.

ACKNOWLEDGMENT

This work is supported by Science Foundation Ireland (grant number 1l/SIRG/I2120).

REFERENCES

1. Hagness, S. C., A. Taflove, and J. E. Bridges, "Three-dimensional FDTD analysis of a pulsed microwave confocal system for breast cancer detection: Design of an antenna-array element," *IEEE Trans. on Antennas and Propagat.*, Vol. 47, No. 5, 783–791, May 1999.
2. Fear, E. C., X. Li, S. C. Hagness, and M. A. Stuchly, "Confocal microwave imaging for breast cancer detection: Localization of

tumors in three dimensions," *IEEE Trans. on Biomed. Eng.*, Vol. 49, No. 8, 812–822, August 2002.

3. Bond, E. J., X. Li, S. C. Hagness, and B. D. V. Veen, "Microwave imaging via space-time beamforming for early detection of breast cancer," *IEEE Trans. on Antennas and Propagat.*, No. 8, 1690–1705, August 2003.
4. Li, X., E. J. Bond, S. C. Hagness, B. D. V. Veen, and D. van der Weide, "Three-dimensional microwave imaging via space-time beamforming for breast cancer detection," *IEEE AP-S International Symposium and USNC/USRI Radio Science Meeting*, San Antonio, TX, USA, June 2002.
5. Xie, Y., B. Guo, J. Li, and P. Stoica, "Novel multistatic adaptive microwave imaging methods for early breast cancer detection," *EURASIP J. Appl. Si. P.*, Vol. 2006, Article ID: 91961, 1–13, 2006.
6. Moriyama, T., Z. Meng, and T. Takenaka, "Forward-backward time-stepping method combined with genetic algorithm applied to breast cancer detection," *Microwave and Optical Technology Letters*, Vol. 53, No. 2, 438–442, 2011.
7. Donelli, M., I. J. Craddock, D. Gibbins, and M. Sarafianou, "A three-dimensional time domain microwave imaging method for breast cancer detection based on an evolutionary algorithm," *Progress In Electromagnetics Research M*, Vol. 18, 179–195, 2011.
8. Klemm, M., I. J. Craddock, J. A. Leendertz, A. Preece, and R. Benjamin, "Improved delay-and-sum beamforming algorithm for breast cancer detection," *International Journal of Antennas and Propagation*, Vol. 2008, Article ID: 761402, 9 Pages, 2008.
9. Sill, J. and E. Fear, "Tissue sensing adaptive radar for breast cancer detection-experimental investigation of simple tumor models," *IEEE Transactions on Microwave Theory and Techniques*, Vol. 53, No. 11, 3312–3319, 2005.
10. Woody, C. D., "Characterization of an adaptive filter for the analysis of variable latency neuroelectric signals," *Medical and Biological Engineering*, Vol. 5, No. 6, 539–554, 1967.
11. Abujarad, F., A. Jostingmeier, and A. Omar, "Clutter removal for landmine using different signal processing techniques," *Proceedings of the Tenth International Conference on Ground Penetrating Radar, GPR*, 697–700, 2004.
12. Verma, P., A. Gaikwad, D. Singh, and M. Nigam, "Analysis of clutter reduction techniques for through wall imaging in UWB range," *Progress In Electromagnetics Research B*, Vol. 17, 29–48, 2009.

13. Zhi, W. and F. Chin, "Entropy-based time window for artifact removal in uwb imaging of breast cancer detection," *IEEE Signal Processing Letters*, Vol. 13, No. 10, 585–588, 2006.
14. Maskooki, A., E. Gunawan, C. B. Soh, and K. S. Low, "Frequency domain skin artifact removal method for ultra-wideband breast cancer detection," *Progress In Electromagnetics Research*, Vol. 98, 299–314, 2009.
15. Piou, J., "A state identification method for 1-D measurements with gaps," *Proc. American Institute of Aeronautics and Astronautics Guidance Navigation and Control Conf.*, 2005.
16. Wax, M. and T. Kailath, "Detection of signals by information theoretic criteria," *IEEE Transactions on Acoustics, Speech and Signal Processing*, Vol. 33, No. 2, 387–392, 1985.
17. Zastrow, E., S. K. Davis, M. Lazebnik, F. Kelcz, B. D. V. Veen, and S. C. Hagness, "Database of 3D grid-based numerical breast phantoms for use in computational electromagnetics simulations," Department of Electrical and Computer Engineering University of Wisconsin-Madison, 2008, [online], available: http://uwcem.ece.wisc.edu/home.htm.
18. Kumar, R. and M. Rattan, "Analysis of various quality metrics for medical image processing," *International Journal*, Vol. 2, No. 11, 2012.